Photoelectron Spectra of $Ar_n \cdot (IHI)^-$ ($n = 0-6$, 12, 20), a Theoretical Study†

José G. López and Anne B. McCoy*

Department of Chemistry, The Ohio State University, Columbus, Ohio 43210

Received: October 18, 2005; In Final Form: December 7, 2005

The effects of the introduction of argon atoms on the photoelectron (PE) spectra of $Ar_n \cdot (IHI)^-$ with $n = 0-6$, 12, and 20 are investigated. Time-independent quantum simulations of the spectra using a rigid cage approximation and allowing the motion of the IHI core are performed. As in our previous classical studies on this system, we find an increase in the confinement of the hydrogen atom motion as the number of argon atoms is increased. Comparison of the quantum and classical descriptions of this confinement provides evidence of the importance of quantum mechanical effects in this system. Three approaches are used to calculate the spectrum of the bare $(IHI)^-$ system. Excellent agreement is found between the simulated peaks in the $\nu_3' = 2$ region using a full three-dimensional quantum simulation of the PE spectrum, those from the corresponding experimental threshold photodetachment spectrum and those obtained by employing an adiabatic separation of the motions of the hydrogen and the iodine atoms. This provides further confirmation that these peaks are the result of motions of the iodine atoms. Simulations of the $Ar_n \cdot (IHI)^-$ PE spectra show a shift of the spectra to lower electron kinetic energies as the number of argon atoms is increased. Similar shifts are found in the experimental spectra and in our previous study of this system using classical trajectory simulations. It is also found that the I−I motion mainly affects the ν_3' spectrum features, whereas the progressions associated with hindered rotor transitions are less affected. Finally, an increase in the intensity of the $\nu_3' = 0$ peak and an accumulation of transitions in the low-frequency hindered rotor region with increasing number of argon atoms are observed.

I. Introduction

Transition state spectroscopy has proven to be a successful approach for investigating the transition state region of bimolecular reactions.[1−3] In particular, anion photodetachment experiments are considered to be among the most powerful techniques for studying this important region of a chemical reaction.[2,4] In this technique, electron photodetachment of a stable anion is used to access the transition state region of the chemical reaction of interest. When the geometry of the anion is similar to that of the transition state complex, the resulting photoelectron (PE) spectrum can provide detailed structural information about the transition state.

In this paper, we continue our investigation of the effects of rare gas solvation on the transition state region in the I + HI reaction. Our main motivation for studying this system comes from the experimental investigations of Neumark and co-workers in which they measured the PE spectra of $Ar_n \cdot (IHI)^-$ with $n = 0-15$[5−7] and previous theoretical investigations performed by Adamovic and Gordon[8] and by us.[9] For bare $(IHI)^-$, Neumark and co-workers observed a well-resolved progression in the PE spectrum that was assigned to the antisymmetric stretch vibration (ν_3') of the IHI complex.[5] They also observed more closely spaced progressions that reflected transitions to symmetric stretch (ν_1') and hindered rotor levels of IHI.[10] Given the 2 orders of magnitude difference in the masses of the hydrogen and iodine atoms, the antisymmetric stretch and hindered rotor motions of IHI correspond to the motions of the hydrogen atom along the I−I axis and around the iodine atoms, respectively. The introduction of argon atoms leads to shifts of the $(IHI)^-$ PE spectrum to lower electron kinetic energies.[6,7] In addition, the introduction of argon atoms leads to a reduction in the hot band structure on the red edge of the PE spectrum. Neumark and co-workers also reported a decrease in the energy difference between the most intense features of the $\nu_3' = 0$ and 2 bands in the spectrum as more argon atoms are introduced to the system.[6,7]

In our previous paper on this system, hereafter referred as paper I, we reported the results of classical trajectory simulations of the transition state dynamics of $Ar_n \cdot (IHI)$ with $n = 0-20$.[9] In that work, we found that the probability that the hydrogen atom will remain near the center of the complex increased as we increased the number of argon atoms in the system. We also found an overall decrease of the average rate of I−I separation after 363 fs with increasing cluster size.

As we move to investigate the quantum dynamics and spectroscopy of the $Ar_n \cdot (IHI)^-$ complexes, we note that previous theoretical studies on the PE spectroscopy of $(XHX)^-$ (X = Br, Cl, and I) and $(BrHI)^-$ have provided useful methodologies for the simulation of the PE spectra of these bihalide anions.[11−21] In terms of the complexes with rare gas atoms, our group has studied the effects of complex formation on the dynamics and spectroscopy of $Ar_n \cdot (IHI)^-$ with $n = 1-5$ using mixed quantum/semiclassical and quantum dynamics approaches.[22−24] Given the heavier mass of the iodine, compared to chlorine, and the larger numbers of argon atoms to be considered, we elect to use time-independent techniques in this study. As we consider the optimal approaches, we draw on the results obtained in our previous classical trajectory studies of the transition state dynamics of $Ar_n \cdot (IHI)$.[9] The fact that the displacements of the heavy atoms were very small compared to that of the hydrogen atom led us to expect that a rigid cage approximation, where the hydrogen atom is allowed to move inside a cage formed by the heavy atoms, would be an appropriate way to investigate the PE spectra of the $Ar_n \cdot (IHI)^-$ complexes quantum mechanically. Here, our

† Part of the special issue "John C. Light Festschrift".

10.1021/jp055962c CCC: $33.50
Published on Web 01/21/2006

first focus will be to explore the validity of the rigid cage approximation and to investigate how well this and other approximations account for the most prominent features in the PE spectra of $(IHI)^-$. Once we are confident in the approaches we turn our attention to the $Ar_n \cdot (IHI)^-$ complexes.

In addition to investigating the validity of the rigid cage approximation and comparing our quantum results to those obtained by classical simulations, we are also interested in using the results of these calculations to obtain PE spectra of $Ar_n \cdot (IHI)^-$ with $n = 0-6$, 12, and 20. By comparing the calculated spectra to the trends in the experimental PE spectra, we hope to gain insights into how the argon atoms affect the PE spectrum of $(IHI)^-$. Specifically, we investigate the motions of the hydrogen and iodine atoms that account for the transitions that are observed in the $Ar_n \cdot (IHI)^-$ PE spectra. Through analysis of the corresponding anion and neutral wave functions we make connections between the introduction of the argon atoms and changes in the experimental $Ar_n \cdot (IHI)^-$ PE spectra brought about by introducing argon atoms to the system. Because we have previously investigated the dynamics of these systems classically, we will also contrast the quantum and classical predictions of the confinement of the hydrogen atom at the center of the neutral clusters with increasing number of argon atoms. This will allow us to develop appropriate computational methodologies that are required in the investigation of the effects of solvating species on the dynamics and spectroscopy of weakly bound systems.

II. Theory

A. Coordinates and Hamiltonian. We use Cartesian and cylindrical coordinates for the quantum calculations of the PE spectra of $Ar_n \cdot (IHI)^-$. In our classical studies of this system, we found displacements of the argon atoms of less than 0.17 Å from their initial positions after 363 fs. On the basis of the near-rigidity of the argon cage, in the present study we constrain the argon atoms to their equilibrium positions in $Ar_n \cdot (IHI)^-$. We align the iodine atoms along the *z*-axis and choose the center of mass of I−I as the origin of the coordinate system used to describe the hydrogen atom dynamics. As a first approximation, we set the interhalogen distance, R_{II}, to 3.88 Å, which is the equilibrium I−I distance in the $(IHI)^-$ potential energy surface used in this work.[17] This approximation is justified by the facts that the main features in the PE spectra of $Ar_n \cdot (IHI)^-$ reflect the motion of the hydrogen atom[5,7] and the slow rate of I−I dissociation found from the classical trajectories reported in paper I. The constrained quantum Hamiltonian is

$$\hat{H} = -\frac{\hbar^2}{2\mu}\left(\frac{\partial^2}{\partial x^2} + \frac{\partial^2}{\partial y^2} + \frac{\partial^2}{\partial z^2}\right) + V(\mathbf{x}) \qquad (1)$$

where μ provides the reduced mass of $H-I_2$, the Cartesian position of the hydrogen atom relative to the center of mass of I−I is specified by (*x*, *y*, *z*), the vector **x** represents the Cartesian positions of all the atoms in this coordinate system, and $V(\mathbf{x})$ is the interaction potential.

In a second set of studies, we relax the constraint on the iodine atoms, allowing them to move while constraining the argon atoms. As Metz and Neumark showed,[17] the motion of the iodine atoms must be considered to account for the quasi-bound reactive resonances observed in the experimental spectrum at 0.520−0.560 eV. For these calculations, the Hamiltonian becomes

$$\hat{H} = -\frac{\hbar^2}{2\mu}\left(\frac{\partial^2}{\partial x^2} + \frac{\partial^2}{\partial y^2} + \frac{\partial^2}{\partial z^2}\right) - \frac{\hbar^2}{2\mu_{I_2}}\frac{\partial^2}{\partial R^2} + V(\mathbf{x}) \qquad (2)$$

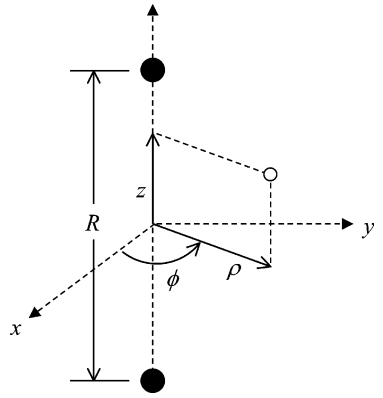

Figure 1. Cylindrical coordinate system for the simulations of the PE spectrum of $(IHI)^-$. Here, the iodine atoms are represented by black circles and the hydrogen atom by a white circle.

where μ_{I_2} is the reduced mass of I−I and *R* is the interiodine distance.

For bare $(IHI)^-$ we use cylindrical coordinates to perform simulations of its PE spectrum with interiodine distance, $R_{II} = 3.88$ Å. The Hamiltonian in these coordinates is

$$\hat{H} = -\frac{\hbar^2}{2\mu}\left(\frac{\partial^2}{\partial \rho^2} + \frac{1}{\rho}\frac{\partial}{\partial \rho} + \frac{1}{\rho^2}\frac{\partial^2}{\partial \phi^2} + \frac{\partial^2}{\partial z^2}\right) + V(\rho,z,R_{II}) \quad (3)$$

where (ρ, ϕ, *z*) represents the position of the hydrogen atom in cylindrical coordinates, Figure 1, and the volume element for integration is $\rho\, d\rho\, d\theta\, dz$.

We also perform a full three-dimensional simulation of the PE spectrum of $(IHI)^-$. Here the Hamiltonian is

$$\hat{H} = -\frac{\hbar^2}{2\mu}\left(\frac{\partial^2}{\partial \rho^2} + \frac{1}{\rho}\frac{\partial}{\partial \rho} + \frac{1}{\rho^2}\frac{\partial^2}{\partial \phi^2} + \frac{\partial^2}{\partial z^2}\right) - \frac{\hbar^2}{2\mu_{I_2}}\frac{\partial^2}{\partial R^2} + V(\rho,z,R) \quad (4)$$

B. Potential Energy Surfaces. Simulations of the PE spectra of $Ar_n \cdot (IHI)^-$ require potential energy surfaces for $Ar_n \cdot (IHI)^-$ and $Ar_n \cdot (IHI)$. For the anion, we construct a potential by combining a $(IHI)^-$ harmonic potential[17] with high quality pairwise additive potentials[24−26] and some three-body interactions.[27,28] The potential for the neutral is similar to the anion. Here we use the LEPS-C potential energy surface of Schatz and co-workers for the I + HI reaction.[15] The form of these potential energy surfaces are described in detail in paper I.

C. Methods. The simulations of the PE spectra of $Ar_n \cdot (IHI)^-$ are performed using the Franck−Condon approximation. In this approximation, the intensities of the peaks are given by the Franck−Condon factor

$$I \propto \left|\left\langle \Psi_0^i \middle| \Psi^f \right\rangle\right|^2 \qquad (5)$$

where Ψ_0^i is the initial $(IHI)^-$ ground-state wave function and Ψ^f is the IHI wave function. The anion ground-state wave function is evaluated by separating the symmetric stretch motion, q_1, from the bending, q_2, and antisymmetric stretch, q_3, motions. The anion wave function in Cartesian coordinates then becomes

$$\Psi_0^i(x,y,z,R) \approx \chi^i_{\nu_1=0}(R)\, \varphi^i_{\nu_2=0,\nu_3=0}(x,y,z) \equiv \chi_0^i(R)\, \varphi^i_{0,0}(x,y,z) \qquad (6)$$

For the simulations of the PE spectrum of $(IHI)^-$ we perform two-dimensional and full three-dimensional evaluations of the neutral wave functions using a discrete variable representation (DVR)[29−32] in cylindrical coordinates. Following the simulation

TABLE 1: Parameters for the DVR Evaluation of the $(IHI)^-$ and IHI Wavefunctions in $Ar_n\cdot(IHI)^-$ and $Ar_n\cdot(IHI)$ (Cartesian Coordinates)

	$n = 0, 6, 20$		$n = 1-5$		$n = 12$	
coordinate	N	range (Å)	N	range (Å)	N	range (Å)
x	22	0.05−2.15	22	0.05−2.15	22	0.05−2.15
y	22	0.05−2.15	44	−2.15−2.15	22	0.05−2.15
z	46	0.05−4.55	46	0.05−4.55	92	−4.55−4.55
R	120	3.31−4.50	120	3.31−4.50	120	3.31−4.50

scheme described by Metz and Neumark,[17] we use a one-dimensional harmonic oscillator basis set for the z coordinate with frequency $\omega_z = 180$ cm^{-1} and DVR points based on the first 45 harmonic oscillator wave functions, $Z_m(z)$, with even values of m. For the ρ coordinate we use the radial portion of a two-dimensional harmonic oscillator with $l_z = 0$, frequency $\omega_\rho = 800$ cm^{-1}, and $N_\rho = 24$ eigenfunctions. For the R coordinate we use a one-dimensional harmonic oscillator basis set centered at $R_c = 3.90$ Å, with frequency $\omega_R = 200$ cm^{-1}, and $N_R = 70$ basis functions for the full three-dimensional simulations. For the adiabatic simulations we use $N_R = 200$ basis functions.

For $n = 0-6$, 12, and 20 we evaluate the neutral wave functions using a DVR in Cartesian coordinates[33] and the adiabatic simulation scheme described by Metz and Neumark.[17] In the adiabatic approximation the motion of the hydrogen atom is separated from the motion of the iodine atoms. The neutral wave function is then

$$\Psi^f(x,y,z,R) \approx \chi^f(R)\, \varphi^f(x,y,z;R) \tag{7}$$

Within this adiabatic approximation, the Franck−Condon factor becomes

$$I \propto \left| \int \mathrm{d}R \left\{ \int \mathrm{d}x \int \mathrm{d}y \int \mathrm{d}z\, \varphi^i_{0,0}(x,y,z)\, \varphi^f_k(x,y,z;R) \right\} \chi^i_0(R)\, \chi^f_{n_k}(R) \right|^2 \tag{8}$$

where $\varphi^f_k(x,y,z;R)$ is the kth hydrogen wave function in IHI, obtained by solving the Schrödinger equation for the hydrogen atom motion at specified values of R, and $\chi_{n_k}(R)$ is the nth halogen wave function obtained by solving the Schrödinger equation for the iodine atoms motion on the kth adiabatic potential curve.

The wave functions are represented on a uniformly spaced grid in all the Cartesian calculations. The number of grid points N and the range for each coordinate are listed in Table 1. We take advantage of the $D_{\infty h}$, D_{6h}, and C_{2h} symmetries for the clusters with $n = 0$, 6, and 20, respectively, and only explicitly evaluate the wave functions for positive values of x, y, and z. For clusters with $n = 1-5$, whose molecular symmetry is C_{2v}, and $n = 12$, C_{6v}, we use similar considerations to reduce the number of grid points.

To evaluate the wave functions and energies for $Ar_n\cdot(IHI)$ more efficiently, we only solve the Schrödinger equation for wave functions and energies of the hydrogen atom at $R_k = 3.35 + 0.1k$ Å, where $k = 0-12$. We use the resulting 1500 eigenfunctions as a basis set to setup the Hamiltonian for intermediate values of R between $R_k - 0.04$ and $R_k + 0.05$. The increment between two adjacent intermediate values is 0.01 Å.[34]

III. Results and Discussion

A. Effects of the Argon Atoms on the Hydrogen Atom in $Ar_n\cdot(IHI)$. Given the factor of 100 difference in mass between the hydrogen and iodine atoms, most of the features in the PE spectra of $Ar_n\cdot(IHI)^-$ reflect motions of the hydrogen atom.[5,7] In paper I, we showed that when argon atoms were introduced to the system, the hydrogen atom became confined. In this section, we investigate the effects of the argon atoms on the range of the motion of the hydrogen atom in $Ar_n\cdot(IHI)$ through an analysis of the wave functions obtained by solving the time-independent Schrödinger equation with the Hamiltonian described in eq 1, i.e., within the rigid cage approximation, and using the parameters listed in Table 1.

In Figure 2 we plot the hydrogen wave functions with $\nu'_3 = 0$ and 2. When no argon atoms are present, slices of these wave functions in the yz plane demonstrate free rotations of the hydrogen atom around the iodine atoms and greater amplitudes near the center of the I−I bond, Figure 2a,d. In paper I, we found that when six argon atoms were introduced to the system, they clustered around the I−I axis forming a ring that was perpendicular to this axis and at equal distances from the iodine atoms. This causes a confinement of the $\nu'_3 = 0$, 2 wave functions near the center of the complex, Figure 2b,e. For $n = 20$, the argon atoms completely surround the IHI. This reduces considerably any orbiting motion of the hydrogen atom around the iodine atoms. As a result, a more dramatic localization of the $\nu'_3 = 0$, 2 hydrogen wave functions at the center of the complex is observed, Figure 2c,f.

We quantify this confinement of the hydrogen atom by calculating the fraction of the probability amplitude, obtained from the hydrogen wave function, that is enclosed by a 8 Å^3 cube that is centered at the center of the I−I bond after 363 fs. We choose this time and cube size to allow comparisons with results reported in paper I using classical trajectory simulations. This wave function is evaluated by solving the time-dependent Schrödinger equation with the Hamiltonian described in eq 1. Because the potential is independent of time, the general solution to this equation is

$$\Psi(x,y,z,t) = \sum_n c_n \varphi_n(x,y,z) \mathrm{e}^{-\mathrm{i}E_n t/\hbar} \tag{9}$$

where $\varphi_n(x,y,z)$ and E_n are the hydrogen wave functions and energies that satisfy the time-independent Schrödinger equation with the Hamiltonian described in eq 1. The coefficient c_n represents the overlap with the anion wave function $\varphi^i_{0,0}(x,y,z)$ described in eq 6.

In Figure 3 we plot the results of this analysis of the confinement of the hydrogen atom that are obtained from the quantum simulations. We also plot the corresponding classical fractions reported in paper I. We find a reduction in the fraction of the probability amplitude that is trapped near the center of the I−I bond when $n \leq 2$. This is due to the repulsive interaction between the argon atoms and the hydrogen atom. For $n = 3$ this behavior starts to reverse and for $n = 5$ and 6 a pronounced increase in the fraction of the probability amplitude near the center of the complex is observed. This is the result of the argon atoms reducing the available configuration space through which the hydrogen atom can leave the center of the complex. Although the quantum calculations only involve the motion of the hydrogen atom, for clusters with $n = 0-6$ the classical results follow the same trend as the quantum results. For larger clusters, the quantum results show a reduction of the fraction of the probability amplitude at the center of the complex compared with the $n = 6$ result. For the same cluster sizes, the classical results show an increase of the fraction of the hydrogen atoms being confined at the center of the I−I bond. Classical simulations of the $Ar_n\cdot(IHI)$ dynamics using the rigid cage

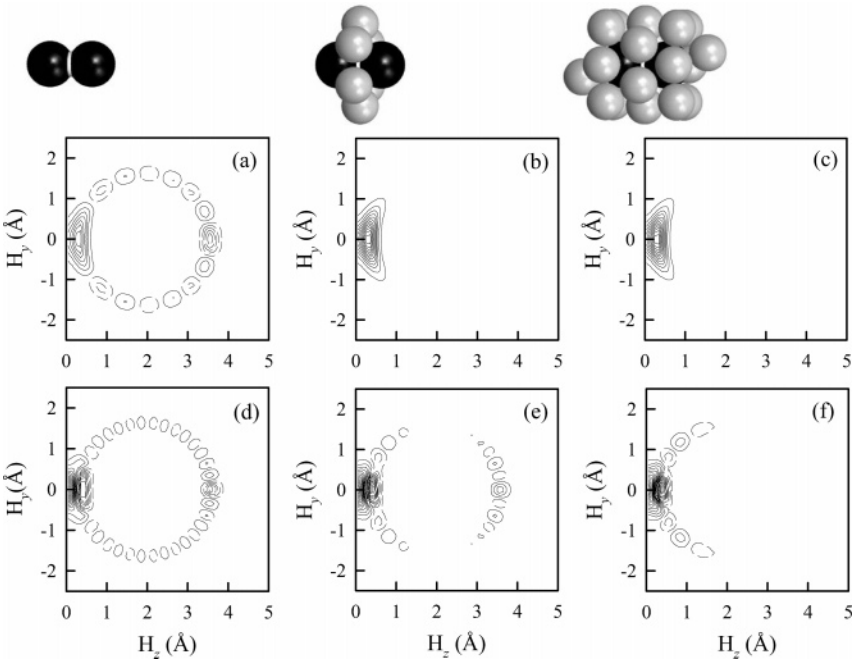

Figure 2. Plots of slices of the hydrogen wave functions in the *yz* plane when $\nu_3' = 0$ (a, b, c) and 2 (d, e, f). Panels (a) and (c) show the wave functions for $n = 0$, (b) and (e) for $n = 6$, and (c) and (f) for $n = 20$ argon atoms. The positive amplitudes are plotted in solid lines and the negative amplitudes are in dashed lines. In all cases, the wave functions are symmetric with respect to reflection in the *xy* plane and only the part of the wave function with $z > 0$ is plotted. To help visualize the positions of the argon atoms, the structure of IHI^-, $Ar_6(IHI)^-$ and $Ar_{20}(IHI)^-$ are depicted above panels (a), (b) and (c), respectively.

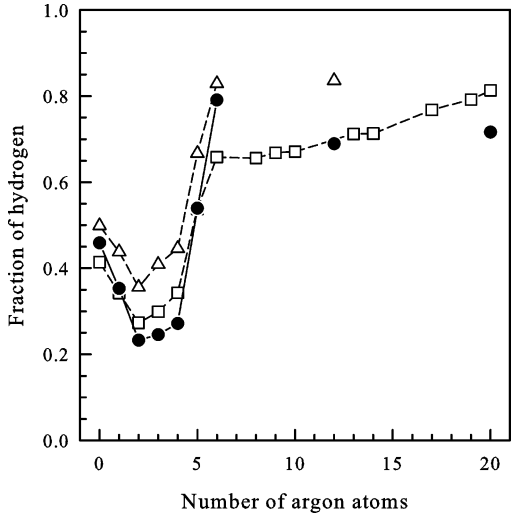

Figure 3. Plots of the fraction of the probability amplitude of the hydrogen wave function (black circles), fraction of the hydrogen atoms using classical trajectory simulations and the rigid cage approximation (white triangles), and using no restrictions on the heavy atoms motion (white squares) that are trapped inside a 8 $Å^3$ cube that is centered at the center of the I−I bond.

approximation, Figure 3, show larger confinement of the hydrogen atom at the center of the complex than that reported in paper I. However, this confinement follows the same trend as that obtained without imposing any restrictions on the heavy atoms motion. Therefore, the discrepancies between the quantum and classical results are attributed to quantum effects.

B. Simulations of the PE Spectrum of $(IHI)^-$. As a first step in our simulations of the PE spectra of $Ar_n \cdot (IHI)^-$, we perform simulations of the PE spectrum of $(IHI)^-$ by two approaches. In the first, we fix the positions of the iodine atoms, and in the second we evaluate the neutral wave functions in their full dimensionality. As noted above, due to the cylindrical symmetry of $(IHI)^-$, if we evaluate these wave functions in cylindrical coordinates only two vibrational degrees of freedom need to be considered when the iodine atoms are constrained, three when all degrees of freedom are considered. Here we investigate the differences between the simulated spectra to determine how appropriate the use of a rigid I−I bond approximation will be for simulations of the larger clusters. Further, through comparisons of our full dimensional simulations with those using the corresponding adiabatic scheme, described by Metz and Neumark,[17] we explore the validity of an adiabatic approximation in the PE spectrum simulations of $Ar_n \cdot (IHI)^-$.

For the calculations of the PE spectra of $Ar_n \cdot (IHI)^-$ we chose our zero in energy to be the energy of the asymptotic channel $I + HI + n$Ar. $E_{Ar_n \cdot (IHI)}$ is related to the electron kinetic energy (eKE) in the experimental PE spectra by

$$\mathrm{eKE} = h\nu - [\Delta E_{\mathrm{ion}}(n) + D_0(\mathrm{IHI})^- + \mathrm{EA}(\mathrm{I}^-) - \mathrm{ZPE}(\mathrm{HI}) + E_{\mathrm{Ar}_n \cdot (\mathrm{IHI})}] \quad (10)$$

where $h\nu$ is the photon energy of the detachment laser (4.66 eV),[7] $\Delta E_{\mathrm{ion}}(n)$ is the binding energy for the loss of the n argon atoms attached to $Ar_n \cdot (IHI)^-$, $D_0(IHI)^-$ is the binding energy of $I^- + HI$, $EA(I^-)$ is the electron affinity of I^-, and ZPE(HI) is the zero-point energy of HI. To illustrate these quantities, in Figure 4 we plot the energy level diagram for the $Ar_n \cdot (IHI)^-/Ar_n \cdot (IHI)$ system.

Figure 5b shows the simulated spectrum of $(IHI)^-$ after fixing the I−I distance to $R_{II} = 3.88$ Å and solving the Schrödinger equation with the Hamiltonian described in eq 3 for the anion and neutral species. We use eq 5 to calculate the intensities of the peaks. Analysis of the simulated spectrum reveals two progressions: a strong progression in the antisymmetric stretch (ν_3') of IHI and a weak progression resulting from transitions to hindered rotor levels of IHI. If we shift the simulated spectrum by 40 meV to lower electron kinetic energies, we see that both progressions are in excellent agreement with some of the peaks in the experimental spectrum.[5] As shown previously by Kubach

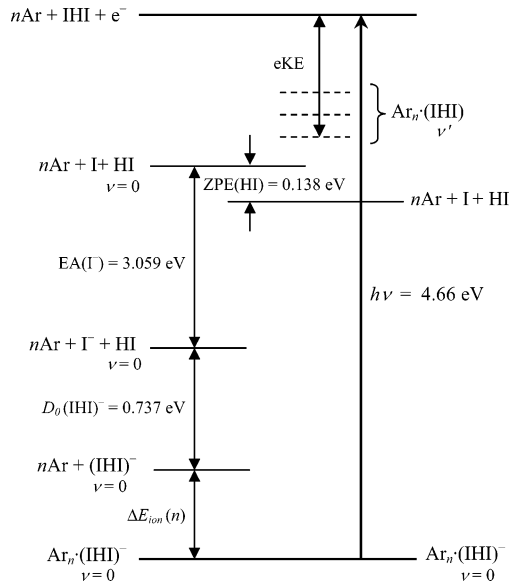

Figure 4. Energy level diagram for the $Ar_n \cdot (IHI)^-/Ar_n \cdot (IHI)$ system. $h\nu$ is the photon energy of the detachment laser,[7] $D_0(IHI)^-$ is the binding energy of $I^- + HI$,[17] EA(I) is the electron affinity of the iodine atom,[35] and ZPE(HI) is the zero-point energy of HI.[36]

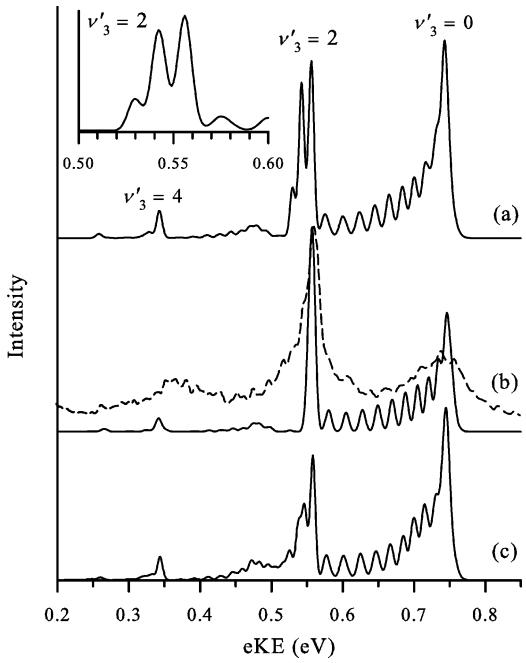

Figure 5. Simulated PE spectra of $(IHI)^-$ (a) using the full dimensionality of the system, (b) after fixing the interiodine distance to R_{II} = 3.88 Å, and (c) using the adiabatic three-dimensional scheme described by Metz and Neumark.[17] The spectra plotted in (a) and (c) have been convoluted with a full-width at half-maximum (fwhm) of 8 meV, and that in (b) with a fwhm of 10 meV. Due to the absence of transitions associated with the I−I motion, a larger stick spacing is observed in the spectrum plotted in (b) and, therefore, a larger fwhm value is used. We selected these resolutions to agree with the experimental resolution of 8−10 meV.[7] All of the simulated spectra have been shifted by 40 meV to lower eKE to facilitate comparisons with the experimental spectra, plotted with dashed lines. The inset shows a progression near $\nu_3' = 2$ that is found in the simulated PE spectrum in its full dimensionality.

and co-workers,[18] comparison of the experimental spectrum and simulated spectrum based on a fixed I−I separation leads to the assignment of most of the features to transitions that involve the hydrogen atom motion. However, there are some peaks that are missing in the simulated spectrum, particularly at high electron kinetic energies and near the $\nu_3' = 2$ and 4 peaks. This is not surprising, given the fact that the motion of the iodine atoms is not considered and some of the peaks near the $\nu_3' = 2$ and 4 peaks have been assigned to quasi-bound reactive resonances associated with the I−I motion.[10] The peaks at electron kinetic energies over 0.8 eV that are observed in the experimental spectrum are the result of transitions from vibrationally excited anions.[6] Because we only consider transitions from the ground state of $(IHI)^-$, these transitions are not found in our simulated spectrum.

For our full dimensional simulations of the PE spectrum of $(IHI)^-$ we evaluate the neutral wave functions by solving the Schrödinger equation with the Hamiltonian described in eq 4. Because the potential for the anion is harmonic, we use separable potentials to evaluate the ground-state wave function of the anion. As described in eq 6, the ground-state wave function for the anion is the product of a two-dimensional wave function for the hydrogen atom and an one-dimensional wave function that describes the I−I motions. The intensities of the peaks in the PE spectrum are calculated using eq 5. In Figure 5a we plot the full-dimensional simulated PE spectrum of $(IHI)^-$. Comparisons between the simulated spectra shown in Figure 5a and b show that when the motion of the iodine atoms is included, the intensities of the peaks associated with the $\nu_3' = 0$ and 4 transitions increase while the progressions associated with hindered rotor transitions are barely affected. This effect on the intensity of some of the peaks can be explained by the fact that the dissociative motion of the iodine atoms occurs along the axis along which the antisymmetric stretch motion, ν_3', of IHI takes place. This situation causes a stronger coupling between these two motions and, therefore, a stronger effect on the peaks associated with the ν_3' motion, while causing a very small effect on the peaks associated with motions of the hydrogen atom that are perpendicular to the I−I axis. These motions correspond to bending motions of IHI and are associated with the hindered rotor transitions observed in the spectrum.

Another difference between the simulated spectra plotted in Figure 5a,b is a new progression near $\nu_3' = 2$ that is found in the full-dimensional simulated spectrum. The inset in Figure 5 shows three peaks at 0.530, 0.542, and 0.556 eV after shifting the simulated spectrum by 40 meV to lower eKE. These are in excellent agreement with the positions of the three partially resolved peaks (0.528, 0.542, and 0.555 eV) that are observed in the experimental threshold photodetachment spectrum of the $\nu_3' = 2$ peak, measured by Neumark and co-workers.[10] Using an adiabatic approximation, Metz and Neumark assigned these peaks to a progression in quasi-bound symmetric stretch states of IHI.[17] Simulation of the $(IHI)^-$ PE spectrum using the adiabatic three-dimensional scheme described by Metz and Neumark,[17] Figure 5c, shows two partially resolved peaks at 0.546 and 0.558 eV. If we use a slightly better resolution for this simulated spectrum, we find another peak at 0.538 meV. When the positions of the three peaks found in our full quantum and the adiabatic simulated spectra are compared with the corresponding experimental peaks, we find better agreement with our full quantum results.

If we focus on the region of the $\nu_3' = 4$ transition, we find good agreement between the full-dimensional simulation and experiment. For example, in both cases there are two peaks, a primary feature and a less intense band at slightly lower electron kinetic energy. In the experimental spectrum, these peaks are split by 11 meV, whereas in the full-dimensional calculated spectrum they are split by 14 meV. When the adiabatic

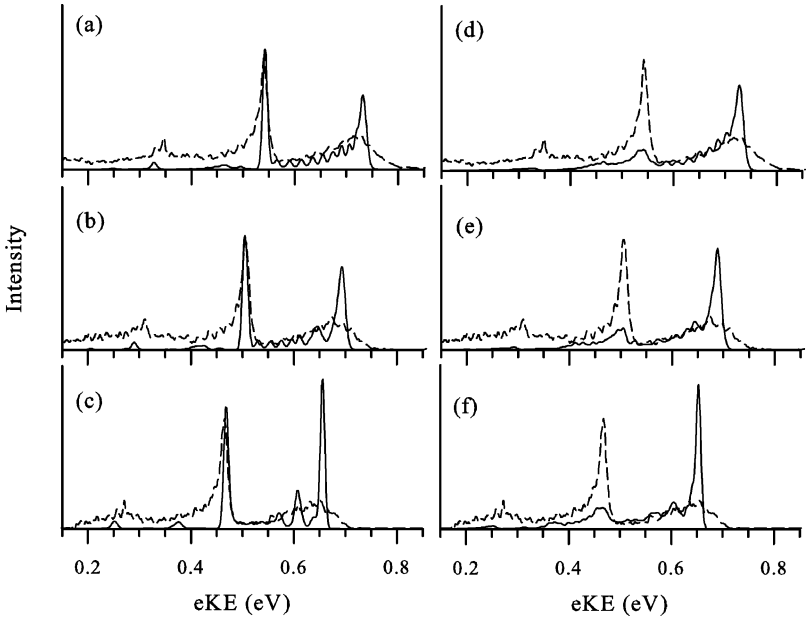

Figure 6. Simulated PE spectra of $Ar_n \cdot (IHI)^-$ with (a) $n = 1$, (b) $n = 3$, and (c) $n = 5$ using a rigid cage approximation, where the hydrogen atom is allowed to move inside a rigid cage formed by the heavy atoms. Simulated PE spectra of $Ar_n \cdot (IHI)^-$ with (d) $n = 1$, (e) $n = 3$, and (f) $n = 5$ using a four-dimensional adiabatic approximation. The spectra in (a), (b), and (c) have been convoluted with a fwhm of 10 meV, and those in (d), (e), and (f) with a fwhm of 8 meV. The spectra with $n = 1$ and 3 have been shifted by 25 and 9 meV to lower eKE, respectively, and those with $n = 5$ have been shifted by 7 meV to higher eKE to agree with the experimental spectra, plotted with dashed lines.

approximation is employed, the intensity of the transition at lower electron kinetic energy is diminished and additional peaks are observed. In this case the splitting between the two largest peaks is 11 meV. As the lower frequency transition is not observed in the spectrum obtained in the rigid cage approximation, it is assigned to an excited state along the I−I stretch coordinate. Combining these results with those discussed for the $\nu_3' = 2$ band we find that we are able to obtain very good agreement between experiment and calculations. This provides further validation of the potential energy surfaces used in these calculations.

Although the general features of the full-dimensional and adiabatic simulated spectra are in good agreement, there are some differences. The most notable difference is the presence of peaks at 0.51 eV in the adiabatic spectrum that are not found in the full-dimensional simulated spectrum. This illustrates that the adiabatic approximation, and the underlying avoided crossings in the adiabatic curves, can cause a spurious increase in the Franck−Condon overlaps between the anion and some neutral hindered rotor wave functions in this region of the spectrum. Comparisons of the peaks associated with the $\nu_3' = 0$ and 2 transitions between the two simulated spectra, show a difference in the relative intensities. We also find a poorer resolution of the quasi-bound I−I peaks near $\nu_3' = 2$ in the adiabatic spectrum. These differences are the result of convergence issues associated with the adiabatic treatment as this treatment requires a denser grid for the DVR than we used for the full-dimensional simulations.[20]

C. Simulations of the PE Spectra of $Ar_n \cdot (IHI)^-$. As we mentioned above, peaks in the PE spectra of $Ar_n \cdot (IHI)^-$ primarily reflect motions of the hydrogen atom. Due to the reduction of symmetry from $D_{\infty h}$ to C_{2v} when one to five argon atoms are introduced to the system, simulations of the PE spectra of $Ar_n \cdot (IHI)^-$ require us to use three coordinates to describe the motion of the hydrogen atom. When the iodine atom motions are considered, the four-dimensional calculations become extremely expensive computationally. In this section we use two approaches that we found to provide good descriptions of the $(IHI)^-$ PE spectrum. In the first, we allow the hydrogen atom to move inside a rigid cage formed by the heavy atoms. In the second, we extend the three-dimensional adiabatic scheme, used by Metz and Neumark[17] to simulate the PE spectrum of $(IHI)^-$, to four-dimensions. All the calculations involved in this section are performed using Cartesian coordinates and the DVR parameters listed in Table 1.

In Figure 6 we plot the simulated PE spectra of $Ar_n \cdot (IHI)^-$ with $n = 1$, 3, and 5 using the two types of approximations, described above. Comparisons of the adiabatic simulations with the corresponding experimental spectra of $Ar_n \cdot (IHI)^-$ show that the use of an adiabatic approximation to perform simulations of these spectra may cause an underestimation of the intensities associated with $\nu_3' = 2$ and 4. When argon atoms are introduced, the molecular symmetry of the system is reduced and more adiabatic curves are required to cover the spectral range. This is particularly problematic in regions where quasi-bound states associated with the I−I motion are expected as the reduced symmetry leads to a large number of avoided crossings. This has the consequence that there is no longer a single curve in the $\nu_3' = 2$ region that is deep enough to support localized states in the I−I stretch coordinate. This can be seen in the plots in Figure 7, where we plot the adiabatic curves at energies near where the quasi-bound states that correspond to $\nu_3' = 2$ present should be located for $Ar \cdot (IHI)$.

Due to the large number of adiabatic curves, the neutral wave functions near $\nu_3' = 2$ are spread out among these curves. This causes an underestimation in the overlap with the anion wave function. Therefore, inclusion of nonadiabatic effects might be required for accurate evaluations of the peak intensities in this region. However, for $n = 1$ the adiabatic approximation gives results for the hindered rotor progressions that are in very good agrement with that using the rigid cage approximation. For $n = 3$, and 5, although the agreement is less good, we find some common features. These are an increase in intensity for the $\nu_3' = 0$ peak and an accumulation of transitions in the low frequency hindered rotor region with increasing number of argon atoms. Due to the fact that the hindered rotor motion of the

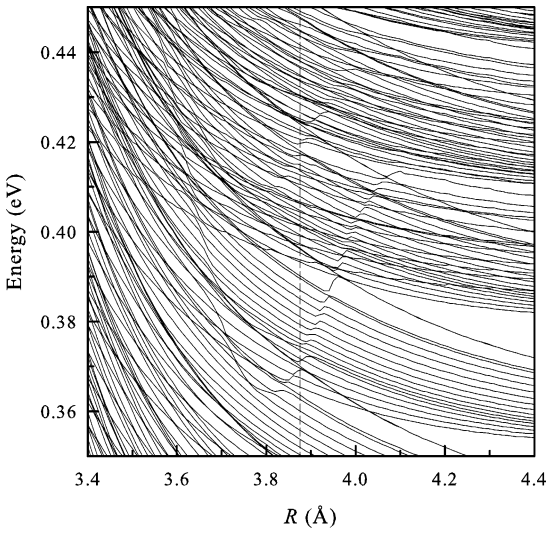

Figure 7. Adiabatic curves for the I + HI reaction with the presence of one argon atom in the region where quasi-bound states associated with the I−I motion and near $\nu_3' = 2$ should be located. The dashed line indicates the interiodine equilibrium distance for $(IHI)^-$, $R_{II} = 3.88$ Å.

hydrogen atom is weakly coupled to the I−I motion, it is not surprising that the adiabatic approximation gives results for these transitions that are similar to those in the rigid cage approximation.

On the basis of the results obtained for the simulated spectra of $Ar_n \cdot (IHI)^-$ with $n = 0$, 1, 3, and 5, we continue our analysis of the effects of argon atoms on the PE spectrum of $(IHI)^-$ using the rigid cage approximation. Figure 8 shows the simulated spectra of $Ar_n \cdot (IHI)^-$ using this approximation. All the spectra are plotted on the same scale and with the same total integrated intensity. When argon atoms are introduced to the system, we find a successive shift of the simulated $Ar_n \cdot (IHI)^-$ PE spectra to lower eKE. Calculations of the stepwise shifts for the $\nu_3' = 2$ peak reveal an increase of about 2 meV in the calculated quantum stepwise spectral shifts compared to the classical $\Delta E_{solv}(n)$ values. As explained in paper I, $\Delta E_{solv}(n)$ is the difference between the solvation energies of the anion and the neutral, where the solvation energies are defined as the dissociation energy of the loss of a single argon atom from $Ar_n \cdot (IHI)^-$ or $Ar_n \cdot (IHI)$. This increase is the result of quantum effects such as changes in the vibrational frequencies of IHI and $(IHI)^-$ and the quantization of the energy levels in IHI. These effects are not considered in the $\Delta E_{solv}(n)$ quantity. Comparisons between the calculated and experimental stepwise spectral shifts show a discrepancy of about 9 meV. As discussed in paper I, this discrepancy is the result of an overestimation of the binding energy of $Ar_n \cdot (IHI)^-$ in our empirical potentials.

Analysis of the simulated ν_3' progression after the introduction of argon atoms reveals very small changes in the intensity of the $\nu_3' = 2$ and 4 bands. In contrast, we find that the intensity of the $\nu_3' = 0$ peak increases with increasing number of argon atoms. The stick spectra, shown in Figure 8, show the presence of more transitions near $\nu_3' = 0$ for the clusters with $n = 1-4$. These transitions contribute to the peak intensity associated with $\nu_3' = 0$. For the clusters with $n = 5$, 6, 12, and 20 the increase in intensity is mainly due to the presence of a single high-intensity transition in this region. Further analysis of the simulated PE spectra of $Ar_n \cdot (IHI)^-$ after introduction of one and two argon atoms, shows a loss of resolution of the peaks associated with the hindered rotor progression. When more argon atoms are present, we find an accumulation of transitions in the low-frequency hindered rotor region. This causes an increase in the intensity of the highest eKE feature and a reduction of the number of peaks associated with the hindered rotor progression as the number of argon atoms is increased. Analysis of the experimental spectra of $Ar_n \cdot (IHI)^-$ revealed a more pronounced hindered rotor structure for the largest clusters.[37] On the basis of these calculations, we observe an accumulation of transitions, as shown in our simulated spectra, which upon convolution result in a series of separated peaks. The structure evolves for $n = 1-6$ but is nearly identical for $n = 6$ and 20. The above observation is consistent with the similarity of the wave functions for these two complexes, plotted in Figure 2b,c and Figure 2e,f. These wave functions also demonstrate an increase in the confinement of the hydrogen atom upon introduction of the argon atoms, which is consistent with the increased peak spacings in the hindered rotor progression as argon atoms are introduced to the system.

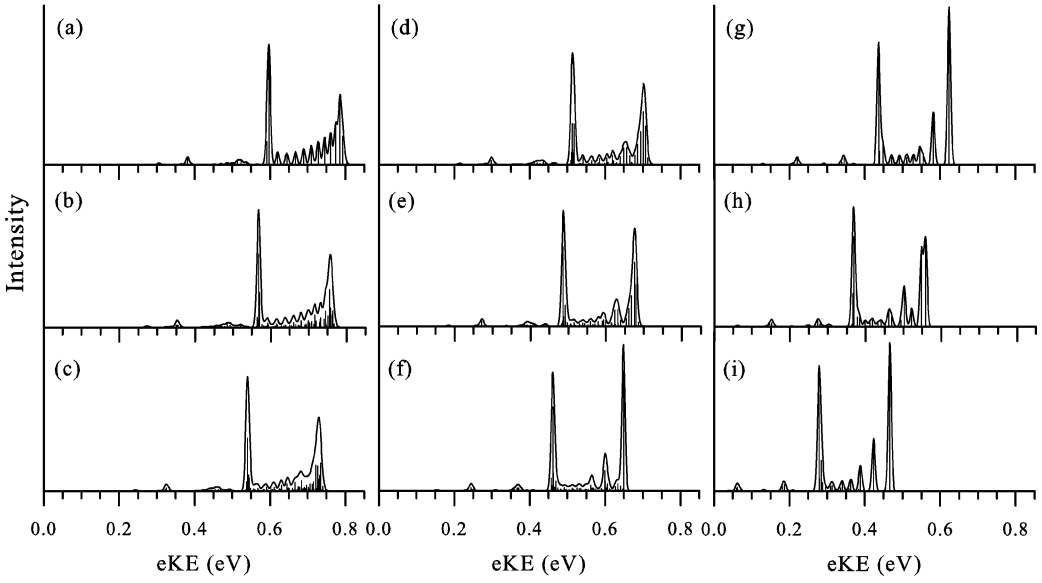

Figure 8. Simulated PE spectra of $Ar_n \cdot (IHI)^-$ with (a) $n = 0$, (b) $n = 1$, (c) $n = 2$, (d) $n = 3$, (e) $n = 4$, (f) $n = 5$, (g) $n = 6$, (h) $n = 12$, and (i) $n = 20$ using a rigid cage approximation, where the hydrogen atom is allowed to move inside a rigid cage formed by the heavy atoms. All the spectra are on the same scale, with the same total integrated intensity, and with a fwhm convolution of 10 meV.

The above changes in the intensities of the $\nu_3' = 0$ and hindered rotor peaks are the result of the loss of cylindrical symmetry and the increasing confinement of the hydrogen atom at the center of the cluster. The reduction of symmetry of the system when a few argon atoms are introduced leads to more allowed transitions. When more than three argon atoms are present, the system becomes more symmetric, and therefore, a reduction of the number of transitions is found. For $n \geq 3$, the confinement of the hydrogen atom wave functions at the center of the complex increases. This causes an increase of the overlap between the anion and neutral wave functions. This, along with the increase of symmetry in the system that reduces the number of transitions, causes an increase in intensity of the $\nu_3' = 0$ peak and more separation between the transitions in the hindered rotor region.

After shifting the full three-dimensional $(IHI)^-$ simulated PE spectrum by 40 meV to lower eKE, we find an overall good agreement of the positions of the peaks when compared to the experimental spectrum, plotted with dashed lines on the same graphs. However, the relative intensities of the peaks are not reproduced that well. As shown by Schatz and co-workers,[15] this is due to deficiencies in the LEPS-C potential. Therefore, further improvement would require us to go beyond a LEPS type potential energy surface for this reaction.

D. Summary and Conclusions. In this paper, we used a time-independent quantum approach to study the effects of rare gas solvation on the transition state region of the I + HI reaction. Specifically, we investigated the effects of argon atoms in the PE spectra of $Ar_n \cdot (IHI)^-$ with $n = 1-6$, 12, and 20 through time-independent quantum calculations. Because PE spectroscopy of $Ar_n \cdot (IHI)^-$ primarily involves the motion of the hydrogen atom, we first investigated the effects of argon atoms on the hydrogen atom wave functions in $Ar_n \cdot (IHI)$. We found an increase in the confinement of the hydrogen wave functions that correspond to $\nu_3' = 0$ and 2 when the number of argon atoms is increased. Analysis of the fraction of the probability amplitude for the hydrogen atom that is trapped at the center of the complex after $t = 363$ fs, showed an excellent agreement with the corresponding classical fractions for cluster with $n = 0-6$. Some discrepancies for the larger clusters were found. These are the result of quantum effects, most likely the increase in the energy of the system brought about by the additional confinement of the hydrogen atom.

On the basis of the classical results that were reported in paper I, we performed simulations of the PE spectra of $Ar_n \cdot (IHI)^-$ using two types of approximations. In the first, we fixed the positions of all the heavy atoms and only considered the motion of the hydrogen atom. In the second, we considered the motion of the IHI core after fixing the positions of the argon atoms. We found that the motion mainly affects the ν_3' spectrum features. Analysis of the results of simulations of the PE spectrum of the bare $(IHI)^-$ system in its full dimensionality provided additional confirmation that the peaks near the $\nu_3' = 2$ are the result of transitions to quasi-bound states associated with the motion.[17] Finally, comparisons between the experimental PE spectra of $Ar_n \cdot (IHI)^-$ and those obtained by using an adiabatic approximation with $n \geq 1$ showed that this approximation may lead to an underestimation of the intensities of the peaks near $\nu_3' = 2$ and 4. Because the trends we observe are similar in the adiabatic and rigid cage approximations, we believe that these results are robust. It is clear, though, that to fully reproduce the spectrum, nonadiabatic effects will need to be included in the calculations of these intensities.

Acknowledgment. We thank Professor Robert Lucchese of Texas A&M University for providing us with the codes to evaluate the Ar-HI potential and Professor Dan Neumark of the University of California, Berkeley, for providing us with the data for the experimental spectra, plotted in Figures 5 and 6. We also thank the National Science Foundation through Grant numbers CHE-0200968 and CHE-0515627.

References and Notes

(1) Brooks, P. R. *Chem. Rev.* **1988**, *88*, 407.
(2) Neumark, D. M. *Annu. Rev. Phys. Chem.* **1992**, *43*, 153.
(3) Polanyi, J. C.; Zewail, A. H. *Acc. Chem. Res.* **1995**, *28*, 119.
(4) Metz, R. B.; Bradforth, S. E.; Neumark, D. M. *Adv. Chem. Phys.* **1992**, *81*, 1.
(5) Weaver, A.; Metz, R. B.; Bradforth, S. E.; Neumark, D. M. *J. Phys. Chem.* **1988**, *92*, 5558.
(6) Liu, Z.; Gómez, H.; Neumark, D. M. *Chem. Phys. Lett.* **2000**, *332*, 65.
(7) Liu, Z.; Gómez, H.; Neumark, D. M. *Faraday Discuss.* **2001**, *118*, 221.
(8) Adamovic, I.; Gordon, M. S. *J. Phys. Chem. A* **2004**, *108*, 11042.
(9) López, J. G.; McCoy, A. B. *J. Phys. Chem. A* **2005**, *109*, 1272.
(10) Waller, I. M.; Kitsopoulos, T. N.; Neumark, D. M. *J. Phys. Chem.* **1990**, *94*, 2240.
(11) Schatz, G. C. *J. Chem. Phys.* **1989**, *90*, 4847.
(12) Schatz, G. C. *J. Chem. Phys.* **1989**, *90*, 3582.
(13) Bowman, J. M.; Gazdy, B. *J. Phys. Chem.* **1989**, *93*, 5129.
(14) Schatz, G. C. *J. Phys. Chem.* **1990**, *94*, 6157.
(15) Schatz, G. C.; Sokolovski, D.; Connor, J. N. L. *Faraday Discuss. Chem. Soc.* **1991**, *91*, 17.
(16) Engel, V. *J. Chem. Phys.* **1991**, *94*, 16.
(17) Metz, R. B.; Neumark, D. M. *J. Chem. Phys.* **1992**, *97*, 962.
(18) Nguyen Vien, G.; Rougeau, N.; Kubach C. *Chem. Phys. Lett.* **1993**, *215*, 35.
(19) Skodje, R. T. *Annu. Rev. Phys. Chem.* **1993**, *44*, 145.
(20) McCoy, A. B.; Gerber, R. B.; Ratner, M. A. *J. Chem. Phys.* **1994**, *101*, 1975.
(21) Kaledin, A.; Skokov, S.; Bowman, J. M.; Morokuma, K. *J. Chem. Phys.* **2000**, *113*, 9479.
(22) McCoy, A. B. *J. Chem. Phys.* **1995**, *103*, 986.
(23) McCoy A. B. In *Advances in Classical Trajectory Methods*; Hase W. L., Ed.; JAI Press Inc.: Greenwich, CT, 1998; Vol. 3, p 183.
(24) Lavender, H. B.; McCoy, A. B. *J. Phys. Chem. A* **2000**, *104*, 644.
(25) Aziz, R. A.; Slaman, M. J. *J. Chem. Phys.* **1990**, *92*, 1030.
(26) Zhao, Y.; Yourshaw, I.; Reiser, G.; Arnold, C. C.; Neumark, D. M. *J. Chem. Phys.* **1994**, *101*, 6538.
(27) Burcl, R.; Cybulski, S. M.; Szczęśniak, M. M.; Chalasiński, G. *J. Chem. Phys.* **1995**, *103*, 299.
(28) McIntosh, A.; Wang, Z.; Castillo-Chará, J.; Lucchese, R. R.; Bevan, J. W.; Suenram, R. D.; Legon, A. C. *J. Chem. Phys.* **1999**, *111*, 5764.
(29) Light, J. C.; Hamilton, I. P.; Lill, J. V. *Adv. Chem. Phys.* **1985**, *114*, 263.
(30) Whitnell, R. M.; Light, J. C. *J. Chem. Phys.* **1989**, *90*, 1774.
(31) Bačič, Z.; Light, J. C. *Annu. Rev. Phys. Chem.* **1989**, *40*, 469.
(32) Light, J. C.; Carrington, T. *Adv. Chem. Phys.* **2000**, *114*, 263.
(33) Colbert, D. T.; Miller, W. H. *J. Chem. Phys.* **1992**, *96*, 1982.
(34) López, J. G. Ph.D. Thesis, The Ohio State University, Columbus OH, 2005 (unpublished), Chapter 4.
(35) *CRC Handbook of Chemistry and Physics*; CRC Press: Cleveland, OH, 2004.
(36) McQuarrie, D. A.; Simon, J. D. *Physical Chemistry: a Molecular Approach*; University Science Books: Sausalito, CA, 1997.
(37) Neumark, D. M. *Phys. Chem. Commun.* **2002**, *5*, 76.